Mon. Not. R. Astron. Soc. **000**, 1–12 (2014) Printed 2 July 2014 (MN LATEX style file v2.2)

Dark energy measurements with SKA HI galaxy surveys

S. Yahya[1]∗, M. Silva[2,3], M. Santos[1,2], P. Okouma[1,4,5], R. Maartens[1,6] and B. Bassett[4,5,7]

[1]*Physics Department, University of the Western Cape, Cape Town 7535, South Africa*
[2]*CENTRA, Instituto Superior Tecnico, Technical University of Lisbon, Lisboa 104900, Portugal*
[3]*Department of Physics & Astronomy, University of California, Irvine, CA 92697, USA*
[4]*African Institute for Mathematical Sciences, Muizenberg, Cape Town 7945, South Africa*
[5]*Department of Mathematics & Applied Mathematics, University of Cape Town, Cape Town 7701, South Africa*
[6]*Institute of Cosmology & Gravitation, University of Portsmouth, Portsmouth PO1 3FX, United Kingdom*
[6]*South African Astronomical Observatory, Cape Town, South Africa*

2 July 2014

ABSTRACT

We use Fisher forecasting and semi-analytical simulations of neutral hydrogen (HI) to predict the performance of Square Kilometer Array (SKA) HI galaxy surveys in measuring dark energy parameters. Measurements of the tangential and radial components of the Baryon Acoustic Oscillation (BAO) length scale over a range of redshifts are the basis for constraints on the dark energy equation of state, the rate of growth of structure and the curvature of the Universe.

Key words: cosmology : radio surveys - galaxy power spectrum - baryonic oscillations - dark energy

1 INTRODUCTION

The acoustic oscillation scale in the CMB temperature anisotropies is also imprinted in the galaxy correlations. This Baryonic Acoustic Oscillation (BAO) scale encodes the angular diameter distance $D_A(z)$ (tangential BAO scale) and the Hubble parameter $H(z)$ (radial BAO scale). One of the key science aims of the SKA is to probe dark energy via surveys of the HI galaxy distribution. These surveys will use the HI 21cm emission line (the hyperfine transition) to detect HI galaxies – detection of the line itself directly gives the redshift of the galaxy. The huge volumes that will eventually be covered by SKA HI galaxy surveys will allow for high-precision measurement of the BAO feature in the radial and tangential directions and at different cosmological redshifts.

The expected performance of these SKA surveys in constraining dark energy was investigated by (Abdalla et al. 2009). Here we update those results, using improved modeling of the number density and bias of the HI galaxy distribution.

THE SKA

The noise associated to the flux measured by the interferometer is assumed Gaussian with a r.m.s given approximately by

$$S_{\rm rms} \approx \frac{2k_B T_{\rm sys}}{A_{\rm eff}\sqrt{\delta\nu\, t_p}}, \tag{1}$$

for an array with total effective collecting area $A_{\rm eff}$, frequency resolution $\delta\nu$ and observation time per pointing t_p (k_B is the Boltzmann constant). Telescope sensitivities are sometimes quoted in terms of the "System Equivalent Flux Density": SEFD $\equiv 2k_{\rm B}T_{\rm sys}/A_{\rm eff}$ or just "A over ": $A_{\rm eff}/T_{\rm sys}$. The effective collecting $A_{\rm eff}$ is usually 70% to 80% of the actual array total area depending of the efficiency of the system. Note that the expression above gives the flux sensitivity per resolution beam (not to confuse with the dish primary beam or telescope field of view). The equivalent brightness temperature uncertainty is

$$\sigma_T = \frac{S_{\rm rms}c^2}{2k_B\nu^2(\delta\theta)^2}, \tag{2}$$

where $\delta\theta$ is the angular resolution of the interferometer. The total temperature is

$$T_{\rm sys} = T_{\rm inst} + T_{\rm sky} \tag{3}$$

∗E-mail:sahbayahya@gmail.com

with $T_{\rm sky} \approx 60\,(300\,{\rm MHz}/\nu)^{2.55}$ K and $T_{\rm inst}$ the instrument temperature which is usually higher than the sky temperature above 300 MHz.

For typical instrument specifications, the single-dish noise r.m.s can be written as:

$$S_{\rm rms} = 368\,\mu{\rm Jy}\left(\frac{T_{\rm sys}}{20\,{\rm K}}\right)\times \left(\frac{25,000\,{\rm m}^2}{A_{\rm eff}}\right)\left(\frac{0.01{\rm MHz}}{\delta\nu}\right)^{1/2}\left(\frac{1{\rm h}}{t_{\rm p}}\right)^{1/2}. \quad (4)$$

For a given survey area ($S_{\rm area}$) we will need $S_{\rm area}/(\theta_{\rm B})^2$ pointings where $(\theta_{\rm B})^2$ is the telescope field of view with the full width at half maximum of the beam, given by (in radians)

$$\theta_{\rm B} \approx \frac{1.22\lambda}{\sqrt{(A_{\rm dish})}}, \quad (5)$$

where $A_{\rm dish}$ is the effective area of each dish. The time per pointing t_p is then related to the total integration time $t_{\rm tot}$ through

$$t_p = t_{\rm tot}\frac{(\theta_{\rm B})^2}{S_{\rm area}}. \quad (6)$$

This will increase the time per pointing at the lowest frequencies. Note that in the table below, following what is in the SKA baseline document we use instead

$$\frac{\theta_{\rm B}}{1{\rm deg}^2} \approx \frac{\pi}{4}\left(\frac{66\lambda}{D}\right)^2. \quad (7)$$

Also, the computed phased array feed (PAF) beams are assumed constant across the band instead of going as λ^2 as above so that the time per pointing is also fixed. Table 1 summarizes the specifications for each telescope, and Table 2 summarizes the specifications for each survey (see Bull et al. (2014)).

2 HI GALAXY SURVEYS

For HI redshift galaxy surveys, the key inputs are (Abdalla et al. 2009) the r.m.s. sensitivity ($S_{\rm rms}$), the detection threshold (n_σ), the telescope field of view and the assumed model for HI evolution.

2.1 HI galaxy redshift distribution

To calculate the HI galaxy number density and bias as a function of flux r.m.s, we used the S^3-SAX simulations[1]. For the detection of a galaxy, we required that at least two points on the HI line are made, that is, the width of the line has to be larger than 2× the assumed frequency resolution of the survey. The idea is to get some information on the typical line double peak expected from HI galaxies due to their rotation. This in principle will remove any galaxy that is seen "face on" as it will show just a narrow peak. More evolved source detection methods can be explored, to avoid spurious detections due to RFI, we will keep this simple approach for now. A signal to noise of 10 is then required for the detection of a galaxy.

Using the S^3-SAX database, we used the following variables and prescription to detect HI galaxies:

- $z_{\rm A}$ is the apparent redshift (including Doppler correction).
- Set experiment spectral resolution to $dV = 2.1(1+z_{\rm A})$ [Km/s]. This corresponds to a frequency resolution of 0.01 [MHz] which is what has been assumed for the sensitivity calculations.
- $w_{\rm P}$ [Km/s] is line width between the two horns of the HI-line profile (already corrected for the galaxy inclination), we take only galaxies where $w_{\rm P}/2 > dV$.
- $v_{\rm HI}$ [Jy Km/s] is the velocity-integrated line flux of the HI-line, for each galaxy we get flux $= v_{\rm HI}/w_{\rm P}$ and we take only galaxies where flux $> 10 \times S_{\rm rms}/\sqrt{(w_{\rm P}/dV)}$.

In order to be as general as possible we didn't try to match completely the $S_{\rm rms}$ used in the query to the above survey specs. Instead we are giving results for several values so that a simple interpolation can be used if we decide to change the survey specs. In particular, if we decide to use a 5σ cut instead of a 10σ, it is just a question of looking for the $S_{\rm rms}$ that is half the survey value (see Table 2).

To obtain the bias, the detected galaxies were put in a box, for which the power spectrum of the number counts was calculated. The bias squared was then taken as the ratio of that power spectrum to the dark matter one at $k = 0.2$ h/Mpc. The SAX-sky simulation consists in a mock observing cone with galaxies and their properties. This simulation was built to add HI and CO properties to the galaxies obtained by De Lucia & Blaizot (2007) using the millennium simulation Springel et al. (2005). The millennium simulation has a box size of 500 h^{-1} Mpc and its galaxies are available at 64 fixed time steps from redshifts 127 to 0. In order to properly emulate the light cone, the SAX-sky simulation used only part of each box of the millennium simulation as is described in Obreschkow et al. (2009). Therefore, the boxes at fixed redshifts with HI properties which can be obtained from the SAX-sky simulation are considerable smaller than 500 h^{-1} Mpc in the line of sight direction.

To be able to use the simulation output at any given redshift, we use the formula of Obreschkow & Rawlings (2009) to fit the simulated dN/dz data points from S^3-SAX:

$$\frac{dN/dz}{1{\rm deg}^2} = 10^{c_1}z^{c_2}\exp\left(-c_3 z\right), \quad (8)$$

where c_i are free parameters. Fig. 1 shows the fitted curves and the data points. The fitted parameters are given in Table 3.

2.2 Galaxy bias from simulation

To obtain the bias, the detected galaxies were put in a box, for which the power spectrum of the number counts was calculated. The bias squared was then taken as the ratio of that power spectrum to the dark matter one at $k = 0.2$ h/Mpc. The initial box for the simulation was

[1] http://s-cubed.physics.ox.ac.uk/s3_sax

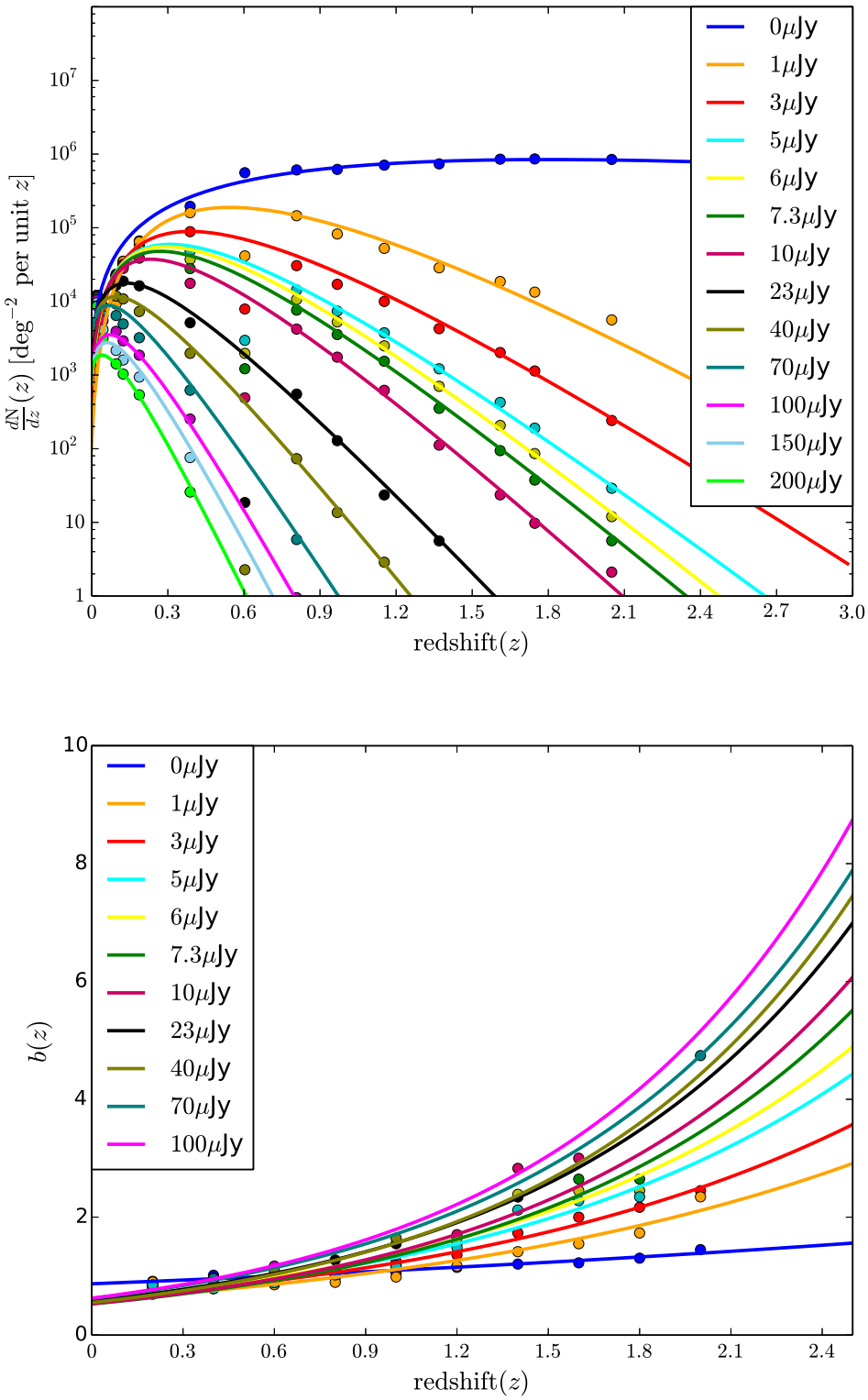

Figure 1. Upper panel: Dependence of the HI galaxy redshift distribution dN/dz (units: deg^{-2}). Note that the numbers are for different $S_{\rm rms}$ which will correspond to a given galaxy flux cut according to the procedure described in the text. Curves are the fits according to Eq. (8) and dots are from the S^3-SAX simulation. Lower Panel: HI galaxy bias for different $S_{\rm rms}$. Note that above 70 μJy values for high redshifts are purely extrapolations. However, this has little impact as at high z shot noise will dominate for these sensitivities.

Telescope	Band [MHz]	z	$T_{\rm inst}$ [K]	$N_{\rm dish}$	$D_{\rm dish}$ [m]	$A_{\rm eff}$ [m^2]	Beam [deg^2] [1]	SEFD [Jy]	$S_{\rm rms}$ [μJy] [2]
ASKAP	700 - 1800[5]	(0) - 1.03	50[9]	36	12.0	3,257	30[4]	42.4	4996
MeerKAT	900 - 1670	(0) - 0.58	20	64	13.5	5,955	1.0	9.27	1093
SKA1-Sur	650 - 1670[3]	(0) - 1.19	30	60	15.0	8,482	18[4]	9.77	1151
SKA1 - Mid	950 - 1760	(0) - 0.50	20	190	15	26,189	0.75	2.1	247
SKA1-Sur+ASKAP	650 - 1670[5]	(0) - 1.19	30[5]	96	–	11,740	18[4]	9.1	832
SKA1-Mid+MK	950 - 1670	(0) - 0.50	20	254	–	32,144	0.8	1.72	202
SKA2	500 - 1200[6]	0.18 - 1.84	20	250	50[7]	400,000	30[8]	0.14	16

Table 1. Telescope configurations. [1] This is the primary beam (FoV) calculated at the center of the band. It changes as λ^2. For the combined telescopes, the smallest beam of the two telescopes is used. [2] Flux rms for a frequency interval of 0.01 MHz and 1 hour integration using eq. 4. [3] Only 500 MHz instantaneous bandwidth. [4] PAF beams assumed constant across the band. [5] Assuming that ASKAP PAFs will be replaced to meet the SKA1-Sur band and instrument temperature of 30K. Assuming that only band 2 will be initially deployed. [6] Band only indicative - can be changed. [7] These should be stations (dense aperture arrays). [8] Assuming multi-beaming to obtain large field of view.

Telescope	Band [MHz]	Beam [deg^2]	$S_{\rm area}$ [deg^2]	t_p [hours]	$S_{\rm rms}$ [μJy][4]
ASKAP[3]	700 - 1800	30	5,000	60	645
MeerKAT	900 - 1670	1.67[1]	5,000	3.34[1]	598[2]
SKA1-Sur[3]	650 - 1670	18	5,000	36	192
SKA1-Mid	950 - 1760	1.38[1]	5,000	2.76[1]	149[2]
SKA1-Sur+ASKAP[3]	700 - 1670	18	5,000	36	139
SKA1-Mid+MK	950 - 1670	1.38[1]	5,000	2.76[1]	122[2]
SKA2[3]	500 - 1200	30	30,000	10	5

Table 2. Survey specifications. We assume a total observation time of 10,000 hours. The flux rms is calculated for a frequency interval of 0.01 MHz. Values were calculated at the target frequency of 1.0 GHz, except for SKA1-Sur band 1 which has an upper limit of 900 MHz. [1] The beam and time per pointing (t_p) are assumed to change as $(\frac{1.0\,\rm GHz}{\nu})^2$ across the band. [2] The flux rms is assumed to change as $\frac{\nu}{1.0\,\rm GHz}$ across the band. [3] The beam, time per pointing and flux rms are assumed constant across the band.

500 Mpc/h, but this was further reduced along the line of sight to avoid cosmic evolution. This puts a problem on the bias extraction since we cannot efficiently use modes below $k \sim 0.1$ h/Mpc. For high flux r.m.s, the number of galaxies is low and the shot noise dominates up to very small ks. In the cosmic variance dominated case the error on the bias squared is just $\Delta b^2 \sim b^2/\sqrt{N}$ with the number of modes $N \sim [4\pi k^2 \delta k]/[(2\pi)^3/{\rm V}]$, δk is the k-bin used and V the volume of the box. The conclusion is that for high flux values the results should be taken as only an indication, in particular for bias above $S_{\rm rms} = 20\mu$Jy. The cosmological analysis should compare results for different fiducial values and fully marginalize over the bias and number counts. The simulated data points are shown in Fig. 1 for different $S_{\rm rms}$ sensitivities. We use an exponential function to fit a galaxy bias $b(z)$ to the simulated data:

$$b = c_4 \exp(c_5 z). \tag{9}$$

Values of the fitted parameters for each r.m.s sensitivity are given in Table 4.

3 THEORETICAL ANALYSIS

The Hubble parameter $H(z) = H_0 E(z)$ and angular diameter distance $D_A(z)$ are given by

$$E = \sqrt{\Omega_M (1+z)^3 + \Omega_K (1+z)^2 + \Omega_{\rm de}\mathcal{F}}, \tag{10}$$

$$D_A = \frac{1}{H_0\sqrt{-\Omega_K}(1+z)} \sin\left(\sqrt{-\Omega_K}\int_0^z \frac{dz'}{E(z')}\right), \tag{11}$$

where $\Omega_{\rm de} = 1 - \Omega_M - \Omega_K$, the dark energy is described by

$$\mathcal{F}(z) = \exp\int_0^z \frac{3[1+w(z')]}{1+z'}dz', \quad w = \frac{p_{\rm de}}{\rho_{\rm de}}, \tag{12}$$

and Ω_M is the matter density ($\Omega_{\rm cdm} + \Omega_b$).

$H(z)$ and $D_A(z)$ are related directly to the comoving size of the BAO feature along and across the line of sight:

$$s_\parallel(z) = \frac{c\Delta z}{H(z)}, \quad s_\perp(z) = (1+z)D_A(z)\Delta\theta. \tag{13}$$

The redshift extent Δz and angular size $\Delta\theta$ of the BAO feature are the observables. In the absence of redshift-space distortions (RSD), we have

$$s_\parallel = s_\perp = s, \tag{14}$$

where s is the comoving acoustic horizon, defined at the drag

Table 3. Values of the fitted parameters of Eq. (8), for different $S_{\rm rms}$.

$S_{\rm rms}$ [μJy]	c_1	c_2	c_3
0	6.21	1.63	0.90
1	7.33	3.02	5.34
3	6.91	2.38	5.84
5	6.77	2.17	6.63
6	6.84	2.23	7.13
7.3	6.76	2.14	7.36
10	6.64	2.01	7.95
23	6.02	1.43	9.03
40	5.74	1.22	10.58
70	5.62	1.11	13.03
100	5.63	1.41	15.49
150	5.48	1.33	16.62
200	5.00	1.04	17.52

Table 4. Values of the fitted parameters of Eq. (9), for different $S_{\rm rms}$.

$S_{\rm rms}$ [μJy]	c_4	c_5
0	0.8695	0.2338
1	0.5863	0.6410
3	0.6003	0.7135
5	0.5884	0.8076
6	0.5908	0.8455
7.3	0.5275	0.9385
10	0.5312	0.9745
23	0.5751	0.9993
40	0.5512	1.0417
70	0.6193	1.0179
100	0.6248	1.0554

epoch. Then observations determine H and D_A separately. In order to parametrize deviations from the simplest (vacuum energy) model of DE ($w = -1$), we use (Chevallier & Polarski 2001; Linder 2003)

$$w(z) = w_0 + w_a \frac{z}{(1+z)}. \tag{15}$$

In this work, we assume a fiducial cosmological model with cosmological parameters

$$h = 0.73,\ \Omega_{\rm cdm} = 0.24,\ \Omega_b = 0.042,\ \Omega_K = 0.0,$$
$$w_0 = -1,\ w_a = 0.0,\ n_s = 1. \tag{16}$$

3.1 Forecasting method

To predict the expected uncertainties in the cosmological parameters measured by the SKA, we use the Fisher forecasting method. The Fisher matrix is

$$F_{ij} \simeq \sum_n \frac{1}{(\Delta x_n)^2} \frac{\partial x_n}{\partial \theta_i} \frac{\partial x_n}{\partial \theta_j}, \tag{17}$$

where θ_i are the cosmological parameters, x_n are the data and Δx_n are the expected uncertainties on the data, which depend on the design of the experiment. The Fisher matrix can be expressed in terms of the observed redshift-space power spectrum P^z and the number density of galaxies n:

$$F_{ij} = \int_{-1}^{1} d\mu \int_{k_{\rm min}}^{k_{\rm max}} \frac{k^2 dk}{8\pi^2} \frac{\partial P^z}{\partial \theta_i} \frac{\partial P^z}{\partial \theta_j} \frac{V_{\rm survey}}{[P^z + n^{-1}]^2}. \tag{18}$$

The real-space power spectrum P is related to P^z by

$$P^z(k,\mu) = R(\mu,k)P(k), \tag{19}$$
$$R(\mu,k) = (1+\beta\mu^2)^2 \exp\left(-k^2\mu^2\Sigma_z^2\right). \tag{20}$$

Here $\mu = \vec{k}\cdot\vec{e}/k$, and $\vec{e}$ is the line-of-sight direction. The linear RSD parameter β is given in terms of the growth rate f by (Komatsu et al. 2009)

$$\beta(z) = \frac{f(z)}{b(z)}, \quad f(z) = -\frac{d\ln D(z)}{d\ln(1+z)}, \tag{21}$$

where D is the growing mode of matter perturbations, normalized so that $D \to (1+z)^{-1}$ at high z. Nonlinear RSD are modelled by the exponential damping term, where

$$\Sigma_z = \frac{\sigma_z(1+z)}{H(z)}, \tag{22}$$

and σ_z is the error on redshift. The survey volume is given by

$$V_{\rm survey} = \left(\frac{\pi}{180}\right)^2 S_{area} \int_{z_{\rm max}}^{z_{\rm min}} \frac{dV}{dz}, \tag{23}$$

where dV/dz is differential comoving volume per unit area, in units of h^{-3} Mpc^3 (Hogg 1999).

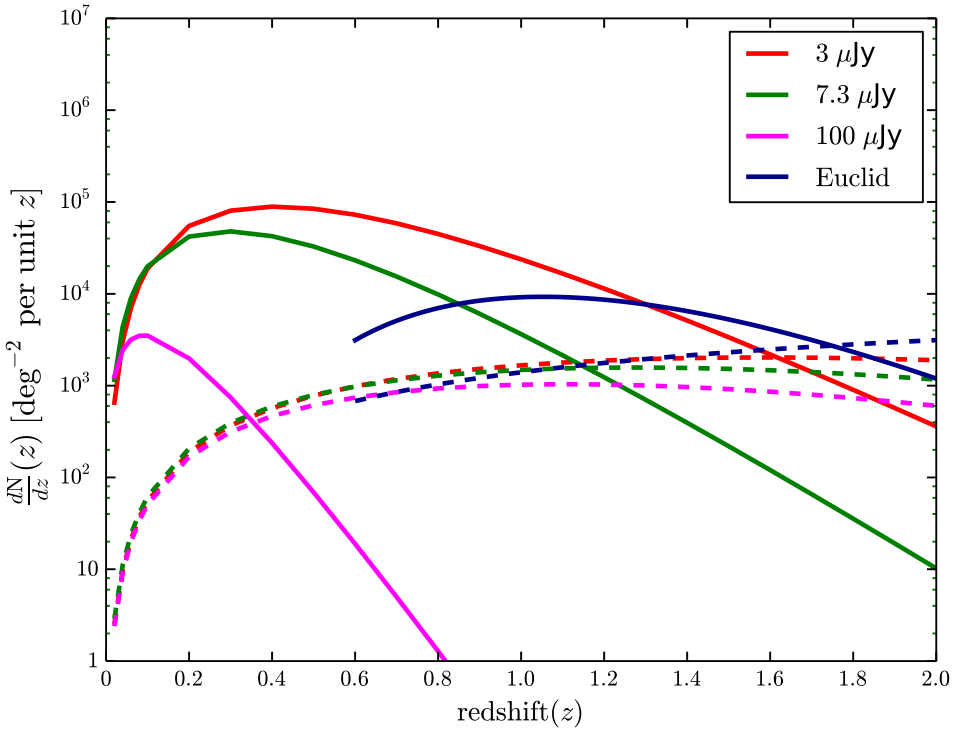

Figure 2. Dashed lines shows the cosmic variance = shot noise for each $S_{\rm rms}$ and for Euclid redshift survey. solid lines shows dN/dz for different sensitivities and for Euclid.

3.2 Wiggles-only method

For forecasting based on the BAO, we can use a simplified approach, that has been called the wiggles-only method (Seo & Eisenstein 2007). The power spectrum in this approach is of the form $P_b \propto \sin(ks)/ks$. The BAO scale is sufficiently large-scale that it is little affected by non-linear matter clustering, non-linear galaxy bias and non-linear redshift distortions. However, the BAO peak is damped and widened by non-linear effects, which can be modelled via non-linearity parameters $k_{\rm S}$, $\Sigma_\perp$ and $\Sigma_\parallel$:

$$P_b = \sqrt{8\pi^2}A_0P_{0.2}\frac{\sin ks}{ks} \times \exp\left[-\left(\frac{k}{k_{\rm S}}\right)^{1.4} - \frac{k^2}{2}\left\{(1-\mu^2)\Sigma_\perp^2 + \mu^2\Sigma_\parallel^2\right\}\right], \quad (24)$$

where

$$k_{\rm S} = 1.6(\Omega_b h^2)^{0.52}(\Omega_{\rm cdm}h^2)^{0.73}\left[1+(10.4\Omega_{\rm cdm}h^2)^{-0.95}\right], \quad (25)$$

and

$$\Sigma_\perp = \Sigma_0 D, \quad \Sigma_\parallel = \Sigma_0(1+f)D. \quad (26)$$

Here $A_0 = 0.5817$ is a normalization factor and $P_{0.2}(z)$ is galaxy power at $k = 0.2h\,{\rm Mpc}^{-1}$ and redshift z. $\Sigma_\perp$ is the r.m.s. displacement across and $\Sigma_\parallel$ is the r.m.s. displacement along the line of sight, and $\Sigma_0 = 12.4h^{-1}\,{\rm Mpc}$ for a cosmology with $\sigma_8 = 0.9$.

If we assume that s is well measured from CMB observations, then the errors on $s_\perp$ and $s_\parallel$ are virtually equivalent to the errors on $D_A(z)$ and $H(z)$. We follow Seo & Eisenstein (2007) and choose

$$\theta_1 = \ln s_\perp^{-1}, \quad \theta_2 = \ln s_\parallel. \quad (27)$$

Then the Fisher matrix evaluated around the fiducial cosmology with $s_\perp = s_\parallel = s$, is given by:

$$F_{ij} = \int_{-1}^{1} d\mu \int_0^\infty k^2 dk \frac{V_{\rm survey}}{[P^z + n^{-1}]^2} \times \left[A_0P_{0.2}R\frac{\partial P_b}{\partial \ln(ks)}\right]^2 \frac{\partial \ln(ks)}{\partial\theta_i}\frac{\partial \ln(ks)}{\partial\theta_j}. \quad (28)$$

3.3 Constraints on the BAO

The measurements of the BAO scale are constrained by two types of errors, cosmic variance and shot noise. Shot noise reflects the limits on reconstructing the matter distribution from galaxy surveys, and is inversely proportional to the number of galaxies at a given survey volume. Upcoming surveys such as the SKA will limit shot noise.

Cosmic variance which is the uncertainty that results from observing only part of the universe at a specific time, limits our statistical knowledge on a cosmological scale. Shot noise and cosmic variance are equal when $nP_{0.2} = 1$.

Abdalla et al. (2009) predict that the full SKA2 survey,

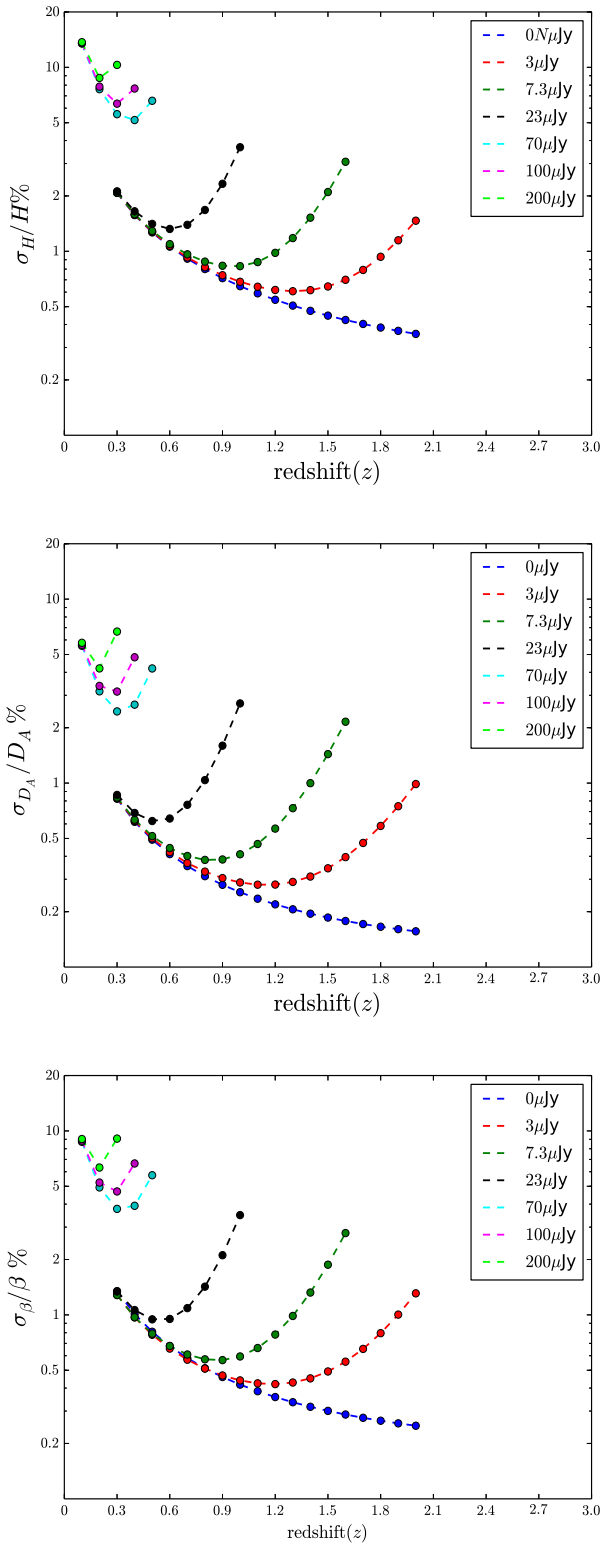

Figure 3. Top: fractional error (%) on the radial component ($\sigma_H/H\%$) . Middle: fractional error (%) on the tangential component ($\sigma_{D_A}/D_A\%$). Bottom: the fractional error (%) on β ($\sigma_\beta/\beta\%$).

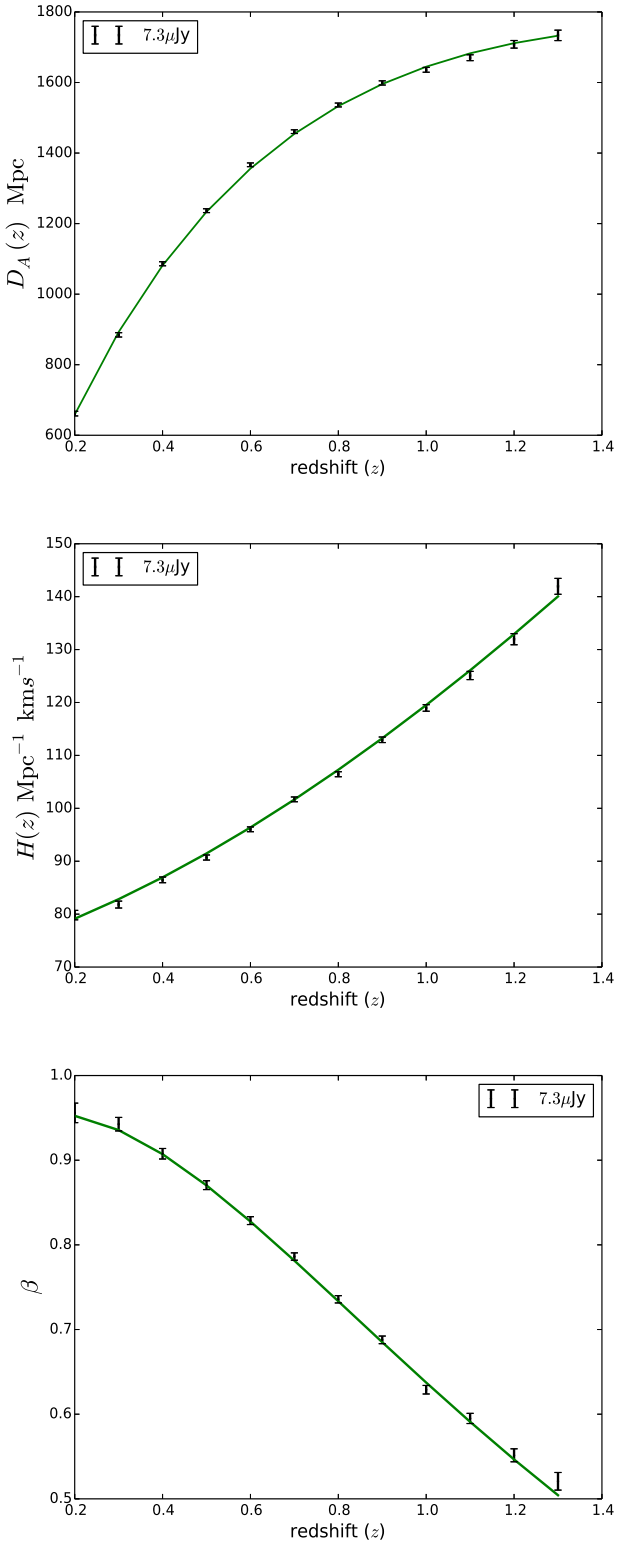

Figure 4. Simulated data points using the errors on Fig. 3 for SKA2 ($S_{\rm rms} = 7.3\mu$Jy): $D_A(z)$ (top), $H(z)$ (middle) and $\beta(z)$ (bottom).

up to $z \sim 1.4$, will be dominated by cosmic variance. Fig. 2 shows that cosmic variance is dominant up to $z \sim 1.8$ and the effect of the bias is clear.

4 RESULTS

Our work considers the SKA, and looks at the Euclid galaxy redshift survey for comparison.

4.0.1 SKA

When we forecast for the SKA1, we consider different possibilities of $S_{\rm rms}$;

- 70μJy as the best case scenario,
- 100μJy as a realistic case ,
- and 200μJy as a pessimistic case.

The sky coverage area for SKA1 ~ 5000 deg^2, see Table 2. Similarly, we forecast for SKA2, with different $S_{\rm rms}$,

- 3μJy as the best case scenario,
- 7.3μJy as a realistic case,
- and 23μJy as a pessimistic case.

SKA2 will have a sky coverage of $30000\,\mathrm{deg}^2$, see Table 2.

For all cases (SKA1 and SKA2) $k_{\rm max} = 0.5h\,\mathrm{Mpc}^{-1}$ and $k_{\rm min} = 10^{-3}h\,\mathrm{Mpc}^{-1}$.

We create redshift bins between 0.01 and 2.0, and for each $S_{\rm rms}$ case the maximum redshift limit, z_{max} is different. z_{max} is set by setting the minimum value for $n(z)$ to $10^{-5}\ h^3\mathrm{Mpc}^{-3}$. Where the redshift bins have a number density less than this limit it does not improve the estimation of error in the Fisher matrix. Tables B1 and B2 show each case of $S_{\rm rms}$ maximum redshift.

4.0.2 Euclid

The Euclid survey is supposed to be a combination between a galaxy survey and a weak lensing survey. To compare the performance of the SKA with other upcoming surveys, we consider the Euclid redshift galaxy survey using the reference case described in Amendola et al. (2013).

4.0.3 0 Noise case

We also consider another general case, for all of the cases mentioned above (4.0.2 and 4.0.1), we assume the number density is infinite, $1/n(z) \sim 0$.

4.1 Errors on D_A and $H(z)$

Using the 2×2 Fisher matrix defined in Eq. (28), the errors on $\ln D_A(z)$ and $\ln H(z)$ are computed (Seo & Eisenstein 2007):

$$\sigma_{\ln D_A} = \sqrt{(F^{-1})_{11}}, \quad \sigma_{\ln H} = \sqrt{(F^{-1})_{22}}. \tag{29}$$

In the case where the tangential and radial BAO scales are assumed to be equal, the error in $\ln R$ can be computed using (Seo & Eisenstein 2007):

$$\sigma^2_{\ln R} = \frac{\sigma^2_{\ln D_A}\left(1-r^2\right)}{1 + 2r\sigma_{\ln D_A}/\sigma_{\ln H} + \sigma^2_{\ln D_A}/\sigma^2_{\ln H}}, \tag{30}$$

where

$$r = \frac{F_{12}}{\sqrt{F_{11}F_{22}}}. \tag{31}$$

Fig. 3 shows the fractional percentage error on the tangential component ($\sigma_H/H\%$), the radial component ($\sigma_{D_A}/D_A\%$) and the linear RSD parameter ($\sigma_\beta/\beta\%$) for both cases SKA1 and SKA2.

In order to indicate how minimal the uncertainty for the SKA2 measurements will be, we produced simulated data points in the given redshift range using the fractional errors for $S_{\rm rms} = 7.3\mu$Jy (one of SKA2 cases), the results are shown in Fig. 4.

4.2 Error propagation to β

From the uncertainty of $\ln R$ in Eq. (30), we can use the propagation of error rule to find the uncertainty of β, assuming that the error contribution from $\Sigma_z \approx 0$:

$$\sigma_\beta = \frac{(1+\mu^2\beta)^2}{2\mu^2}\sigma_{\ln R(\mu)}. \tag{32}$$

The errors in β versus redshift for different sensitivities are shown in Fig. 3.

4.3 Error propagation to dark energy equation of state

We parameterize $w(z)$ via Eq. (15), and propagate the errors in $D_A(z)$ and $H(z)$, Eq. 18, to the cosmological parameters using:

$$\tilde{F}_{\alpha\beta} = \sum_{ij} \frac{\partial\theta_i}{\partial\theta_\alpha}\frac{\partial\theta_j}{\partial\theta_\beta}F_{ij}. \tag{33}$$

where $\theta_i = (\ln D_A, \ln H)$ and $\theta_\alpha = (w_0, w_a, \Omega_{\rm cdm}, \Omega_b, \Omega_K, h)$, for detailed calculations see Eq. A1.

4.3.1 Adding priors

Forecasting the errors for the cosmological parameters w_0, w_a, $\Omega_{\rm cdm}$, Ω_b, Ω_K and h, is achieved by adding a diagonal prior matrix, derived from Plank's prior matrix (Amendola et al. 2013), to the SKA Fisher matrix, see Table 4.3.1.

We also add prior information about the angular diameter distance out to $z = 1090$ from the last scattering surface (LSS) using Eq. (A2):

$$\frac{\sigma_{D_A(1090)}}{D_A(1090)} = 0.001 \tag{34}$$

Our predictions have been based on three assumptions:

-	n_s	w_0	w_a	Ω_b	Ω_K	$\Omega_{\rm cdm}$	h	σ_8
n_s	1.995792e+05	-3.736675e+04	-1.049368e+04	1.399776e+06	5.586439e+05	1.911997e+06	-7.651819e+04	-2.238062e+03
w_0	-3.736675e+04	1.839286e+05	5.165256e+04	-7.420507e+06	-3.987583e+06	-1.252519e+07	1.324383e+06	-4.515591e+02
w_a	-1.049368e+04	5.165256e+04	1.450555e+04	-2.083896e+06	-1.119830e+06	-3.517442e+06	3.719258e+05	-1.268110e+02
Ω_b	1.399776e+06	-7.420507e+06	-2.083896e+06	3.649438e+08	1.585996e+08	5.661366e+08	-5.168785e+07	3.203389e+04
Ω_K	5.586439e+05	-3.987583e+06	-1.119830e+06	1.585996e+08	8.705355e+07	2.705270e+08	-2.917404e+07	1.884381e+04
$\Omega_{\rm cdm}$	1.911997e+06	-1.252519e+07	-3.517442e+06	5.661366e+08	2.705270e+08	9.116277e+08	-8.940715e+07	6.346286e+04
h	-7.651819e+04	1.324383e+06	3.719258e+05	-5.168785e+07	-2.917404e+07	-8.940715e+07	9.889490e+06	-1.018381e+04
σ_8	-2.238062e+03	-4.515591e+02	-1.268110e+02	3.203389e+04	1.884381e+04	6.346286e+04	-1.018381e+04	1.517096e+04

Table 5. Plank's prior matrix corresponds to the cosmological parameters of interest.

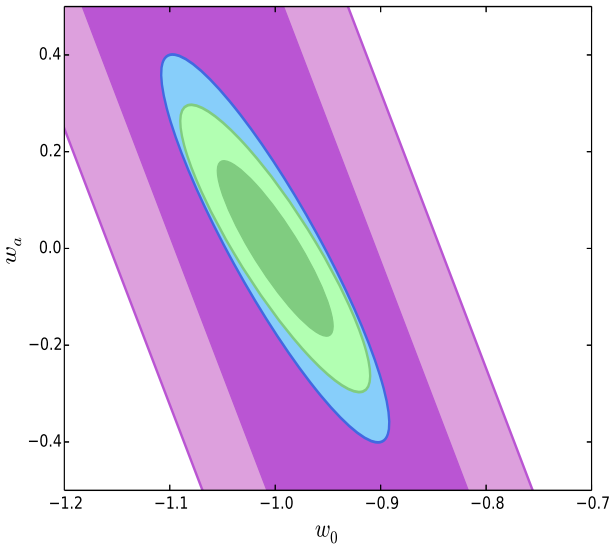

Figure 5. Projected constraints 1σ and 2σ confidence limits on the dark energy parameters w_0 and w_a for SKA1+Planck priors with $S_{\rm rms} = 100\mu$Jy (purple), SKA2+Planck priors with $S_{\rm rms} = 7.3\mu$Jy (green) and Euclid galaxy survey + Planck priors (blue).

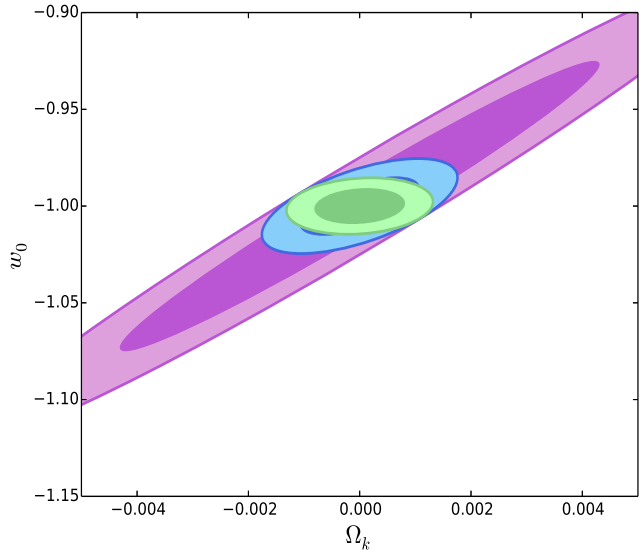

Figure 6. Projected constraints on w_0 and Ω_K, 1σ and 2σ confidence limits for the SKA1+Planck priors where $S_{\rm rms} = 100\mu$Jy (red), for the SKA2+Planck priors where $S_{\rm rms} = 7.3\mu$Jy (green) and for Euclid galaxy survey+Plank priors (blue).

- Non-flat universe: When we estimate the errors for $w_0, w_a, \Omega_{\rm cdm}, \Omega_b, \Omega_K, h$, the Fisher matrix is a 6×6 matrix, see the results in Table 6; The results for $S_{\rm rms} = 100\mu$Jy (SKA1) and $S_{\rm rms} = 7.3\mu$Jy (SKA2) are also shown in Fig. 5.

- Flat universe: We fixed $\Omega_K = 0$, and forecast the errors for $w_0, w_a, \Omega_{\rm cdm}, \Omega_b, h$, therefore the Fisher matrix is a 5×5 matrix, the results are shown in Table 7.

- We assume a non flat universe and constant $w = -1$, then Fisher matrix is 5×5. Table 8 shows the errors on the cosmological parameters and Fig. 6 shows the constraints on w and Ω_K for $S_{\rm rms} = 100\mu$Jy and 7.3μJy.

Note that for all cases we added Planck priors and the prior information about the angular diameter distance to the SKA Fisher matrices.

Table 6. Shows different $S_{\rm rms}$, $\sigma_{D_A}/D_A\%$ and $\sigma_H/H\%$, and the corresponding error values of $w_0,\ w_a,\ \Omega_{\rm cdm},\ \Omega_b, \Omega_K,\ h$. Last column shows FoM of the SKA.

Setup	$S_{\rm rms}$ [μJy]	$\sigma_{D_A}/D_A\%$	$\sigma_H/H\%$	σ_{w_0}	σ_{w_a}	$\sigma_{\Omega_{\rm cdm}}$	σ_{Ω_b}	σ_{Ω_K}	σ_h	DETF FoM
SKA1 (5000 deg^2)	70	1.4	2.82	0.5584	3.09	0.007	7.174e-03	0.030	0.020	07
	100	1.9	3.79	1.0636	6.06	0.015	1.467e-02	0.062	0.041	03
	200	2.9	5.75	2.1059	12.24	0.030	3.048e-02	0.129	0.086	01
SKA1 (5000 deg^2)	0 noise	0.13	0.31	0.0324	0.11	0.001	5.385e-04	0.001	0.003	492
SKA2 (30000 deg^2)	3	0.09	0.19	0.0248	0.07	0.001	5.195e-04	0.001	0.003	910
	7.3	0.14	0.30	0.0362	0.12	0.001	5.773e-04	0.001	0.003	496
	23	0.28	0.58	0.0727	0.32	0.001	8.699e-04	0.003	0.004	157
SKA2 (30000 deg^2)	0 noise	0.05	0.13	0.0178	0.05	0.001	4.874e-04	0.001	0.002	1460
Euclid (15000 deg^2)	-	0.22	0.40	0.0435	0.16	0.001	5.600e-04	0.001	0.003	327
Euclid (15000 deg^2)	0 noise	0.13	0.29	0.0328	0.12	0.001	5.406e-04	0.001	0.003	462

Table 7. Shows different values of the $S_{\rm rms}$, and the corresponding error values of $w_0,\ w_a,\ \Omega_{\rm cdm},\ \Omega_b,\ h$ where Ω_K is **fixed**. Last column shows FoM of the SKA.

Setup	$S_{\rm rms}$ [μJy]	σ_{w_0}	σ_{w_a}	$\sigma_{\Omega_{\rm cdm}}$	σ_{Ω_b}	σ_h	DETF FoM
SKA1 (5000 deg^2)	70	0.1108	0.40	3.549e-04	3.430e-04	0.002	88
	100	0.1553	0.55	3.558e-04	3.438e-04	0.002	63
	200	0.2612	0.93	3.585e-04	3.467e-04	0.002	37
SKA1 (5000 deg^2)	0 noise	0.0244	0.11	2.035e-04	2.772e-04	0.001	828
SKA2 (30000 deg^2)	3	0.0146	0.06	1.863e-04	2.724e-04	0.001	1762
	7.3	0.0178	0.09	2.290e-04	2.895e-04	0.001	1066
	23	0.0253	0.12	3.103e-04	3.235e-04	0.002	472
SKA2 (30000 deg^2)	0 noise	0.0118	0.05	1.647e-04	2.634e-04	0.001	2609
Euclid (15000 deg^2)	-	0.0347	0.15	2.345e-04	2.893e-04	0.002	489
Euclid (15000 deg^2)	0 noise	0.0268	0.12	2.002e-04	2.757e-04	0.001	763

Table 8. Shows different values of $S_{\rm rms}$ and their corresponding error values of $w, \Omega_K, \Omega_{\rm cdm}, \Omega_b, h$ for the SKA, on this case we assume $w = w_0 = -1$.

Setup	$S_{\rm rms}$ [μJy]	σ_{w_0}	σ_{Ω_K}	$\sigma_{\Omega_{\rm cdm}}$	σ_{Ω_b}	σ_h
SKA1 (5000 deg^2)	70	0.0417	2.409e-03	5.5e-04	6.187e-04	6.194e-04
	100	0.0492	2.835e-03	6.1e-04	6.948e-04	6.212e-04
	200	0.0555	3.194e-03	6.7e-04	7.614e-04	6.232e-04
SKA1 (5000 deg^2)	0 noise	0.0058	5.424e-04	3.4e-04	3.743e-04	6.152e-04
SKA2 (30000 deg^2)	3	0.0048	4.996e-04	3.3e-04	3.695e-04	6.115e-04
	7.3	0.0059	5.302e-04	3.3e-04	3.708e-04	6.123e-04
	23	0.0104	7.087e-04	3.4e-04	3.826e-04	6.135e-04
SKA2 (30000 deg^2)	0 noise	0.0042	4.897e-04	3.3e-04	3.683e-04	6.086e-04
Euclid (15000 deg^2)	-	0.0075	6.049e-04	3.4e-04	3.785e-04	6.164e-04
Euclid (15000 deg^2)	0 noise	0.0059	5.447e-04	3.4e-04	3.749e-04	6.157e-04

4.4 Figure of Merit

We define the figure of merit (FoM) as

$$\mathrm{FoM} = \sqrt{\det(F)}, \tag{35}$$

which is also equivalent to the inverse of the $1-\sigma$ ellipse in units of the area of the unit circle (Bassett et al. 2011; Coe 2009). We used this definition to find the FoM for the flat case and the non-flat case in Tables 6 and 7.

Acknowledgements:
SY thanks Pedro Ferreira for valuable guidance, and for hospitality during her visit to Oxford University where part of this work was done. SY, MS, PO and RM are supported by the South Africa Square Kilometer Array Project and the South African National Research Foundation. RM acknowledges support from the UK Science & Technology Facilities Council (grant ST/K0090X/1).

REFERENCES

Abdalla F. B., Blake C., Rawlings S., 2009, Mon. Not. Roy. Astron. Soc., 401, 743

Ade P., et al., 2013, arXiv: 1303.5076

Amendola L., et al., 2013, Living Reviews in Relativity, 16, 6

Bassett B. A., Fantaye Y., Hlozek H R., Kotze J., 2011, International Journal of Modern Physics D, 20, 2559

Bull P., Ferreira P. G., Patel P., Santos M. G., 2014, arXiv: 1405.1452

Chevallier M., Polarski D., 2001, Int. J. Mod. Phys., D10, 213

Coe D., 2009, arXiv: 0906.4123

De Lucia G., Blaizot J., 2007, Mon. Not. Roy. Astron. Soc., 375, 2

Hogg D. W., 1999, arXiv: astro-ph/9905116

Komatsu E., et al., 2009, Astrophys.J.Suppl., 180, 330

Linder E. V., 2003, ArXiv: 0311403

Obreschkow D., Klöckner H.-R., Heywood I., Levrier F., Rawlings S., 2009, Astrophys. J., 703, 1890

Obreschkow D., Rawlings S., 2009, Astrophys. J., 703, 1890

Seo H.-J., Eisenstein D. J., 2007, Astrophys. J., 665, 14

Shoji M., Jeong D., Komatsu E., 2009, Astrophys. J., 693, 1404

Springel V., et al., 2005, Nature, 435, 629

APPENDIX A: PROPAGATION OF ERROR CALCULATIONS

Partial derivatives of D_A and H with respect to w_0 and w_a are given by (Shoji et al. 2009)

$$
\begin{aligned}
\frac{\partial \ln D_A}{\partial w_0} &= -\frac{3}{2}\Omega_{\rm de}\frac{\int_0^z \ln(1+z')\mathcal{F}(z')E(z')^{-3}dz'}{\int_0^z E(z')^{-1}dz'},\\
\frac{\partial \ln D_A}{\partial w_a} &= -\frac{3}{2}\Omega_{\rm de}\\
&\times \frac{\int_0^z \left\{\ln(1+z') - \frac{z'}{(1+z')}\right\}\mathcal{F}(z')E(z')^{-3}dz'}{\int_0^z E(z')^{-1}dz'},\\
\frac{\partial \ln D_A}{\partial \Omega_{\rm cdm}} &= -\frac{1}{2}\frac{\int_0^z \left\{(1+z')^3 - \mathcal{F}(z')\right\}E(z')^{-3}dz'}{\int_0^z E(z')^{-1}dz'},\\
\frac{\partial \ln D_A}{\partial \Omega_b} &= -\frac{1}{2}\frac{\int_0^z \left\{(1+z')^3 - \mathcal{F}(z')\right\}E(z')^{-3}dz'}{\int_0^z E(z')^{-1}dz'},\\
\frac{\partial \ln D_A}{\partial \Omega_K} &= -\frac{1}{2}\frac{\int_0^z \left\{(1+z')^2 - \mathcal{F}(z')\right\}E(z')^{-3}}{\int_0^z E(z')^{-1}dz'}\\
&+ \frac{1}{6}\left(\int_0^z E(z')^{-1}dz'\right)^2,\\
\frac{\partial \ln D_A}{\partial h} &= \frac{1}{h}\\
\frac{\partial \ln H}{\partial w_0} &= \frac{3}{2}\Omega_{\rm de}\ln(1+z)\frac{\mathcal{F}(z)}{E^2(z)},\\
\frac{\partial \ln H}{\partial w_a} &= \frac{3}{2}\Omega_{\rm de}\left\{\ln(1+z) - \frac{z}{(1+z)}\right\}\frac{\mathcal{F}(z)}{g(z)},\\
\frac{\partial \ln H}{\partial \Omega_{\rm cdm}} &= \frac{1}{2}\left\{(1+z)^3 - \mathcal{F}(z)\right\}\frac{1}{E^2(z)},\\
\frac{\partial \ln H}{\partial \Omega_b} &= \frac{1}{2}\left\{(1+z)^3 - \mathcal{F}(z)\right\}\frac{1}{E^2(z)},\\
\frac{\partial \ln H}{\partial \Omega_K} &= \frac{1}{2}\left\{(1+z)^2 - \mathcal{F}(z)\right\}\frac{1}{E^2(z)},\\
\frac{\partial \ln H}{\partial h} &= -\frac{1}{h},
\end{aligned}
$$

where $\mathcal{F}(z)$ and $E(z)$ are given by Eq. (12) and (10) respectively.

We marginalize over H_0, $\Omega_{\rm cdm}$, Ω_b and Ω_K, and we add the distance information from LSS as

$$F^{total}_{\alpha\beta}(z) = F^{LSS}_{\alpha\beta} + F^{gal}_{\alpha\beta}(z), \tag{A1}$$

where we add the angular diameter distance at $z = 1090$ using

$$F^{LSS}_{\alpha\beta} = 10^4 \frac{\partial \ln D_A(z=1090)}{\partial q_\alpha}\frac{\partial \ln D_A(z=1090)}{\partial q_\beta}. \tag{A2}$$

APPENDIX B: FURTHER DETAILS

In the section we show the uncertainty on the values of H and D_A at different redshift bins considering different SKA setups (see Table B1, B2 and B3). Also, the tables show the number of galaxies at each redshift bin.

Table B1. 1st column shows $S_{\rm rms}$ (survey area), where the 2nd column shows the redshift bins. The errors on D_A and H (3rd and 4th column) at different redshift bins. 5th and 6th columns show the percentage error on D_A and $H(z)$ respectively (see Fig. 3).

$S_{\rm rms}$ (Jy)	z	σ_{D_A} [Mpc]	σ_H [Mpc]	$\sigma_{D_A}/D_A\%$	$\sigma_H/H\%$	n(z) [h^3Mpc^{-3}]
3 μJy (30000 deg^2)	0.02	31.70	68.79	39.51	93.55	1.14e-01
	0.04	31.75	35.75	20.25	48.25	1.35e-01
	0.06	31.08	24.20	13.52	32.41	1.42e-01
	0.08	30.35	18.36	10.12	24.40	1.44e-01
	0.1	8.30	4.16	2.27	5.49	1.42e-01
	0.2	8.11	2.41	1.23	3.05	1.13e-01
	0.3	7.40	1.73	0.83	2.08	8.11e-02
	0.4	6.74	1.37	0.62	1.58	5.58e-02
	0.5	6.18	1.17	0.50	1.28	3.76e-02
	0.6	5.72	1.03	0.42	1.07	2.50e-02
	0.7	5.35	0.94	0.37	0.93	1.65e-02
	0.8	5.06	0.88	0.33	0.82	1.08e-02
	0.9	4.86	0.84	0.30	0.74	6.99e-03
	1.0	4.74	0.82	0.29	0.68	4.52e-03
	1.1	4.72	0.81	0.28	0.64	2.90e-03
	1.2	4.81	0.82	0.28	0.62	1.86e-03
	1.3	5.03	0.85	0.29	0.61	1.18e-03
	1.4	5.42	0.91	0.31	0.61	7.50e-04
	1.5	6.05	1.00	0.34	0.64	4.70e-04
	1.6	6.98	1.14	0.40	0.70	3.00e-04
	1.7	8.34	1.35	0.47	0.79	1.90e-04
	1.8	10.30	1.67	0.58	0.93	1.20e-04
	1.9	13.15	2.15	0.75	1.15	7.00e-05
	2.0	17.29	2.88	0.99	1.47	5.00e-05
7.3 μJy (30000 deg^2)	0.02	31.65	68.74	39.45	93.48	2.03e-01
	0.04	31.73	35.73	20.23	48.23	1.95e-01
	0.06	31.08	24.19	13.52	32.41	1.81e-01
	0.08	30.36	18.36	10.13	24.40	1.65e-01
	0.1	8.31	4.17	2.27	5.49	1.50e-01
	0.2	8.13	2.41	1.24	3.05	8.64e-02
	0.3	7.45	1.73	0.83	2.09	4.82e-02
	0.4	6.84	1.38	0.63	1.59	2.66e-02
	0.5	6.35	1.18	0.52	1.29	1.46e-02
	0.6	6.02	1.05	0.44	1.09	7.96e-03
	0.7	5.84	0.98	0.40	0.96	4.34e-03
	0.8	5.86	0.94	0.38	0.88	2.36e-03
	0.9	6.13	0.94	0.38	0.83	1.28e-03
	1.0	6.75	0.99	0.41	0.83	6.90e-04
	1.1	7.85	1.10	0.47	0.87	3.70e-04
	1.2	9.68	1.30	0.57	0.98	2.00e-04
	1.3	12.66	1.65	0.73	1.18	1.10e-04
	1.4	17.46	2.25	1.00	1.52	6.00e-05
	1.5	25.25	3.26	1.44	2.10	3.00e-05
	1.6	37.98	4.99	2.16	3.07	2.00e-05
	1.7	58.92	8.02	3.34	4.69	1.00e-05

Table B2. This table is a continuation of Table B1

$S_{\rm rms}$ (Jy)	z	σ_{D_A} [Mpc]	σ_H [Mpc]	σ_{D_A}/D_A%	σ_H/H%	n(z) [h^3Mpc^{-3}]	$V_{\rm survey}$ [h^{-3}Gpc^3]
23 μJy (30000 deg^2)	0.02	31.56	68.66	39.33	93.37	5.58e-01	
	0.04	31.66	35.71	20.19	48.20	3.20e-01	
	0.06	31.04	24.18	13.50	32.39	2.16e-01	
	0.08	30.34	18.36	10.12	24.40	1.56e-01	
	0.1	8.31	4.17	2.27	5.49	1.17e-01	
	0.2	8.21	2.42	1.25	3.06	3.49e-02	
	0.3	7.70	1.75	0.86	2.12	1.24e-02	
	0.4	7.44	1.43	0.69	1.65	4.72e-03	
	0.5	7.67	1.29	0.62	1.41	1.87e-03	
	0.6	8.70	1.27	0.64	1.32	7.60e-04	
	0.7	11.08	1.42	0.76	1.39	3.10e-04	
	0.8	15.92	1.80	1.04	1.68	1.30e-04	
	0.9	25.49	2.64	1.60	2.33	6.00e-05	
	1.0	44.58	4.40	2.71	3.68	2.00e-05	
	1.1	82.97	8.13	4.93	6.45	1.00e-05	
70 μJy (5000 deg^2)	0.02	77.27	168.16	96.30	228.68	7.22e-01	
	0.04	77.54	87.46	49.45	118.05	3.06e-01	
	0.06	76.06	59.24	33.08	79.36	1.67e-01	
	0.08	74.43	45.00	24.83	59.81	1.02e-01	
	0.1	20.43	10.22	5.58	13.47	6.55e-02	
	0.2	20.76	6.02	3.15	7.61	1.06e-02	
	0.3	21.90	4.61	2.45	5.56	2.21e-03	
	0.4	28.86	4.49	2.67	5.17	5.10e-04	
	0.5	51.80	6.02	4.20	6.58	1.30e-04	
	0.6	122.61	11.49	9.04	11.93	3.00e-05	
	0.7	346.23	29.29	23.80	28.81	1.00e-05	

Table B3. This table is a continuation of Table B2

$S_{\rm rms}$ (Jy)	z	σ_{D_A} [Mpc]	σ_H [Mpc]	σ_{D_A}/D_A%	σ_H/H%	n(z) [h^3Mpc^{-3}]	$V_{\rm survey}$ [h^{-3}Gpc^3]
100 μJy (5000 deg^2)	0.02	77.41	168.30	96.49	228.87	2.20e-01	
	0.04	77.81	87.59	49.62	118.22	1.09e-01	
	0.06	76.49	59.39	33.27	79.55	6.40e-02	
	0.08	75.06	45.17	25.04	60.03	4.03e-02	
	0.1	20.69	10.28	5.65	13.55	2.63e-02	
	0.2	22.22	6.21	3.37	7.85	4.07e-03	
	0.3	28.08	5.26	3.14	6.35	7.50e-04	
	0.4	52.23	6.67	4.83	7.67	1.50e-04	
	0.5	142.85	13.70	11.58	14.97	3.00e-05	
	0.6	495.58	41.52	36.55	43.08	1.00e-05	
200 μJy (5000 deg^2)	0.02	77.42	168.30	96.50	228.88	2.11e-01	
	0.04	77.98	87.67	49.73	118.33	7.77e-02	
	0.06	76.97	59.55	33.48	79.76	3.78e-02	
	0.08	76.07	45.43	25.38	60.38	2.05e-02	
	0.1	21.21	10.39	5.79	13.70	1.19e-02	
	0.2	27.67	6.93	4.20	8.75	1.16e-03	
	0.3	59.47	8.54	6.66	10.31	1.50e-04	
	0.4	221.75	21.61	20.50	24.85	2.00e-05	